




Benchmarking of Fluorescence Lifetime Measurements using Time-Frequency Correlated Photons

Tobias B. Gäbler *

*Fraunhofer Institute for Applied Optics and Precision Engineering IOF,
Albert-Einstein-Straße 7, 07745 Jena, Germany and*

Abbe Center of Photonics, Friedrich Schiller University Jena, Albert-Einstein-Straße 6, 07745 Jena, Germany



Patrick Then  and Christian Eggeling 

*Institute of Applied Optics and Biophysics and Microverse Imaging Center,
Friedrich Schiller University Jena, Philosophenweg 7, 07743 Jena, Germany and*

Leibniz Institute of Photonic Technology IPHT, Albert-Einstein-Straße 9, 07745 Jena, Germany

Markus Gräfe 

*Institute of Applied Physics, Technical University of Darmstadt,
Schloßgartenstraße 7, 64289 Darmstadt, Germany*

Nitish Jain  and Valerio F. Gili 

Fraunhofer Institute for Applied Optics and Precision Engineering IOF, Albert-Einstein-Straße 7, 07745 Jena, Germany
(Dated: January 16, 2025)

The investigation of fluorescence lifetime became an important tool in biology and medical science. So far, established methods of fluorescence lifetime measurements require the illumination of the investigated probes with pulsed or amplitude-modulated light. In this paper, we examine the limitations of an innovative method of fluorescence lifetime using time-frequency correlated photons generated by a continuous-wave source. For this purpose, we investigate the lifetime of IR-140 to demonstrate the functional principle and its dependencies on different experimental parameters. We also compare this technique with state-of-the-art FLIM and observed an improved figure-of-merit. Finally, we discuss the potential of a quantum advantage.

I. INTRODUCTION

The capability of excitation and measurement of fluorescence light is fundamentally important for research activities in biology, chemistry and medicine. A variety of imaging methods base on fluorescence, starting from single or two-photon microscopy [1] via fluorescence correlation spectroscopy [2] towards super-resolution methods like stimulated emission depletion microscopy [3, 4]. All these methods have benefits as well as drawbacks, which specialize them for different applications.

One of the highly specialized methods is fluorescence lifetime imaging microscopy (FLIM). It represents a very valuable tool for investigations on the chemical environment of fluorescence dyes [5–12]. However, a drawback of fluorescence lifetime measurements in general is the requirement of pulsed light sources or optic modulators. This leads to high risk of photobleaching and more complex optical setups. To avoid these drawbacks is an ongoing research topic.

In 2023, two research groups showed, independently of one another, that fluorescence lifetime measurements are possible by using entangled photon pair sources [13, 14]. Their work provides the basis for a new generation of fluorescence lifetime microscopes using upcoming quan-

tum technologies. In particular, they utilized the time-frequency correlation of entangled photon pairs generated by spontaneous parametric down-conversion (SPDC). In doing so, one photon of this pair excites single-photon fluorescence while the other one triggers the timing measurement. The time difference between the arrivals of heralding photon and the fluorescence photon represents a measure for the fluorescence lifetime.

In this work, we consider different technical aspects of this method of lifetime measurements, like the dependency on the spectrum of entangled photons or heralding efficiencies, to set a framework for its evaluation towards application-oriented implementations. To achieve this goal, we investigate the fluorescence dye IR-140 with photons generated by a SPDC source based on nonlinear waveguides. We further benchmark the results with classical state-of-the-art tools. For this purpose, we will give insights into the methodology of fluorescence lifetime measurements using entangled photons (sec. II), describe our experimental approach (sec. III) and present our results (sec. IV).

II. FUNDAMENTALS

While the measurement of fluorescence spectra provides insights into the electronic structures of matter, fluorescence lifetimes can provide information on the chemical environment and enable the separation of fluo-

* corresponding author: tobias.bernd.gaebler@iof.fraunhofer.de

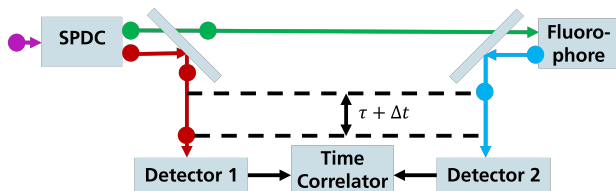


FIG. 1: Principle scheme of FLIM using time-frequency correlated photon pairs generated by SPDC

rophores with similar spectral emission [15, 16]. For the determination of these lifetimes τ , the decay of the fluorescence intensity F over time t after an excitation event will be considered.

$$F(t, \tau) = F_0 \cdot \exp(-t/\tau) \quad (1)$$

F_0 represents the fluorescence intensity at $t = 0$. Due to other processes that occur simultaneously, such as intersystem crossing or internal conversion, apart from fluorescence, observed lifetimes τ contain contributions of all these processes. For this reason, τ is composed by different decay constants k_i

$$\tau = \sum_i k_i^{-1} \quad (2)$$

In general, eq. (2) will be simplified by separation of the fluorescence process with constant k_f and all non-radiative processes with constant k_{nr} . Both constants will be affected by the chemical environment, for example, by temperature, pH-value or concentration [10].

One of the state-of-the-art methods of determining τ is based on pulsed illumination [15]. As the name suggests, pulsed light sources are used to excite the fluorescence. The time delay between an electronic trigger signal, which indicates the generation of a light pulse, and the fluorescence detection is a measure for the duration of the fluorescence process. Because of this direct consideration of time delays, FLIM based on pulsed illumination is referred to time-domain methods. However, the transmission of the trigger signal and the time of flight of excitation photons already introduce a time delay Δt . For this reason, the measured fluorescence signal $\tilde{F}(t, \tau)$ represents a convolution of the real fluorescence decay F and the so-called instrumental response function $IRF(t)$, which contain all time delays Δt caused by the apparatus (eq. (3)).

$$\tilde{F}(t, \tau) = IRF(t) * F(t, \tau) \quad (3)$$

IRF will be measured by replacing the sample by a mirror so that the excitation photons trigger the fluorescence detector.

As shown simultaneously by Harper et al. [13] and Es-hun et al. [14], the principle idea of time-domain FLIM can also be executed by CW light sources. Key ingredient is the usage of time-frequency correlated photon

pairs, for example, generated by spontaneous parametric down-conversion (SPDC). As depicted in fig. 1, the photons of a pair can be spatially separated so that one photon excites the fluorescence dye whereas the other one triggers a time-correlated single photon counting unit (TC-SPC). Because both photons of a pair are generated simultaneously (or more exactly within the Heisenberg uncertainty) during the SPDC process, the measured time difference between heralding and generated fluorescence photon corresponds to fluorescence lifetime τ and the additional time delay Δt introduced by the apparatus.

Nevertheless, since this measurement principle corresponds to the classical time-domain FLIM in essential features, the measured fluorescence decay $\tilde{F}(t)$ can also be described via eq. (3). Using TCSPC, IRF and $\tilde{F}(t)$ appear in form of temporal histograms. Because IRF does not contain any temporal contributions, which lead to an asymmetric histogram, it can be described by a Gaussian distribution given in eq. (4) [17].

$$IRF(t) = \frac{1}{\sqrt{2\pi\sigma_{IRF}^2}} \cdot \exp\left(-\frac{[t - \mu_{IRF}]^2}{2\sigma_{IRF}^2}\right) \quad (4)$$

On the other side, $\tilde{F}(t)$ is asymmetric because of the convolution of a symmetric with an asymmetric function. But the knowledge of eq. (1) and (4) leads to an analytic expression of $\tilde{F}(t)$ [17].

$$\tilde{F}(t, \tau) = \frac{F_0}{2} \cdot \exp\left(\frac{\sigma_{IRF}^2}{2\tau^2}\right) \cdot \exp\left(-\frac{t - \mu_{IRF}}{\tau}\right) \cdot \left[1 + \operatorname{erf}\left(\frac{t - \mu_{IRF} - \sigma_{IRF}^2/\tau}{\sqrt{2\sigma_{IRF}^2}}\right)\right] \quad (5)$$

These two expressions (4) and (5) finally enable the determination of τ from the measurement data as explained later in sec. III B. Exploiting time-frequency correlated photon pairs for fluorescence life time measurements offers another advantage. The excitation wavelength is easily adjustable. A fact that was not yet considered. The base for this forms the momentum and energy conservation during the SPDC process. The wavelengths of the two photons of a generated pair are correlated and depend on the pump wavelength introduced into the nonlinear crystal as well as on its angle [18] or temperature [19, 20]. Since, in particular, the crystal temperature can be easily modified, it may enable an use case for fluorescence lifetime spectroscopy. But to implement this, photon pair sources with narrow SPDC bandwidth are necessary. Typical sources use bulky nonlinear crystals, which show relatively broad bandwidths depending on the length of the crystal [21]. Better performance regarding narrow SPDC bandwidths is shown by photon pair sources based on nonlinear waveguides. Due to selective mode coupling, these sources have much narrower bandwidths [22, 23] together with higher conversion efficiencies [21, 24–26].

Spectroscopic approaches to fluorescence lifetime measurements are usually known as sFLIM (spectrally resolved fluorescence lifetime imaging microscopy) [8–10, 12]. Physical basis for sFLIM is the wavelength dependency of decay constants k_i caused by diverse effects. The most obvious one are the electronic structures of dye molecules which result in characteristic wavelength-dependent absorption and fluorescence behavior of every fluorescence species. However, these electronic structures can be influenced by, for example, chemical bonds to the chemical environment.

III. METHOD

A. Experimental Setup

Our experimental setup consisted of a source of time-frequency correlated photon pairs and a tailor-built microscope. The photon pairs source, shown on the left side of fig. 2, based on a periodically poled lithium-niobate waveguide with a length of 20 mm (AdVR), which was pumped by a CW diode laser with a center wavelength of 405 nm (Toptica iBeam-Smart-405-S-HP). Correlated photons were generated by SPDC type-0 with a center wavelength of 810 nm. Residual pump photons were filtered out by 405 nm-notch (Thorlabs NF405-13) and 750 nm-longpass filters (Thorlabs FELH0750). A detailed description of the key characteristics of this source is given in ref. [25].

The tailor-built microscope, shown on the right side of fig. 2, contained two shortpass dichroic mirrors (Thorlabs DMSP805R) and a microscope objective (Olympus LUC-PLFLN40X). The first dichroic mirror enabled the separation of heralding photons (above 805 nm) and exciting photons (below 805 nm). Heralding photons were coupled by a adjustable collimator (Thorlabs PAF2P-A15B) into a multimode fiber (Thorlabs M123L01). This fiber is connected to a single-photon avalanche detector (Excelitas SPCM-800-42-FC; channel 1). For avoiding the saturation of this detector, the pump power coupled into the waveguide was set to $(27.6 \pm 1.3) \mu\text{W}$ to limit the total number of generated photon pairs. Additional neutral density filters (Thorlabs NUK01) were added in front of the collection of heralding photons to investigate the dependence on heralding efficiency η .

Photons with a wavelength below 805 nm, which passed the first dichroic mirror, were led through the second mirror into the microscope objective and focused on the sample to excite the fluorescence dye. Fluorescence photons emitted with a wavelength above 805 nm are collected by this objective and redirected by the second dichroic mirror into a fiber coupler (Thorlabs PAF2-A7B). Due to the imperfect reflectivity of the dichroic mirrors, an additional 800 nm-longpass filter (Thorlabs FELH0800) was used to prevent that residual heralding or exciting photons are reaching this light path. Fluorescence photons are guided with a multimode fiber

(Thorlabs M123L01) to a second detector (also Excelitas SPCM-800-42-FC; channel 2). Both detectors, channel 1 and 2, are electrically connected to a TCSPC (QuTools QuTag).

As fluorescence sample, the fluorophore IR-140 (Sigma-Aldrich 260932-100MG) was used in a solution with ethanol (Sigma-Aldrich 51976-500-ML-F) with a concentration of 1.3 mmol L^{-1} . This sample was filled into a cuvette (Thorlabs CV1Q035AE) and mounted on a two-axis translation stage (stack of two Thorlabs PT1). On the same stage, a mirror (Thorlabs BB1-E03) was mounted to allow a simple exchange with the sample in the optical path to record the *IRF*.

As explained in sec. II, the temperature dependent recording of the histograms enables a direct correlation to the excitation wavelength λ_0 . This relation between waveguide temperature ϑ and wavelength of time-frequency correlated photons is shown in fig. 3. Due to the conservation of energy and momentum, the described source exhibits a degenerate spectrum at approximately $\vartheta = 62^\circ\text{C}$. Above this temperature, the spectra have two significant peaks with correlated center wavelengths, representing both photons of a pair. For this reason, waveguide temperatures above $\vartheta = 63^\circ\text{C}$ were used exclusively to ensure a clear separation of heralding and exciting photons in all measurements.

B. Data Recording and Processing

The TCSPC was set to a bin width of 2 ps and bin count of $N_t = 5000$ to ensure the complete recording of all histograms with high temporal precision. All histograms of *IRF* and \tilde{F} as well as the single and coincidence counts are measured for different cases: At first, the integration time T was increased from 1 s up to 1 h for a fixed waveguide temperature of $\vartheta = 64^\circ\text{C}$. This case is used to investigate the accuracy of the lifetime determination as it was already shown in ref. [13] (section IV A). Secondly, measurements with different neutral density filters placed in front of the heralding detector (channel 1) for an integration time of $T = 15 \text{ min}$ and a waveguide temperature of $\vartheta = 64^\circ\text{C}$ were executed. The aim of this is the consideration of the effect of heralding efficiency and signal-to-noise ratio on the lifetime determination (section IV B). The last measurement was performed to investigate the possibility of spectroscopic applications (section IV C). For this purpose, the waveguide temperature ϑ was varied between 63.0°C and 70.0°C for a fixed integration time of 15 min.

Because of the long measurement times, TCSPC and temperature controller were controlled automatically by Python codes. These are available in ref. [27]. The post-processing of the histograms was also performed by Python codes in the following way:

1. Elimination of the background of *IRF*(t) and \tilde{F} (t) caused by accidentals

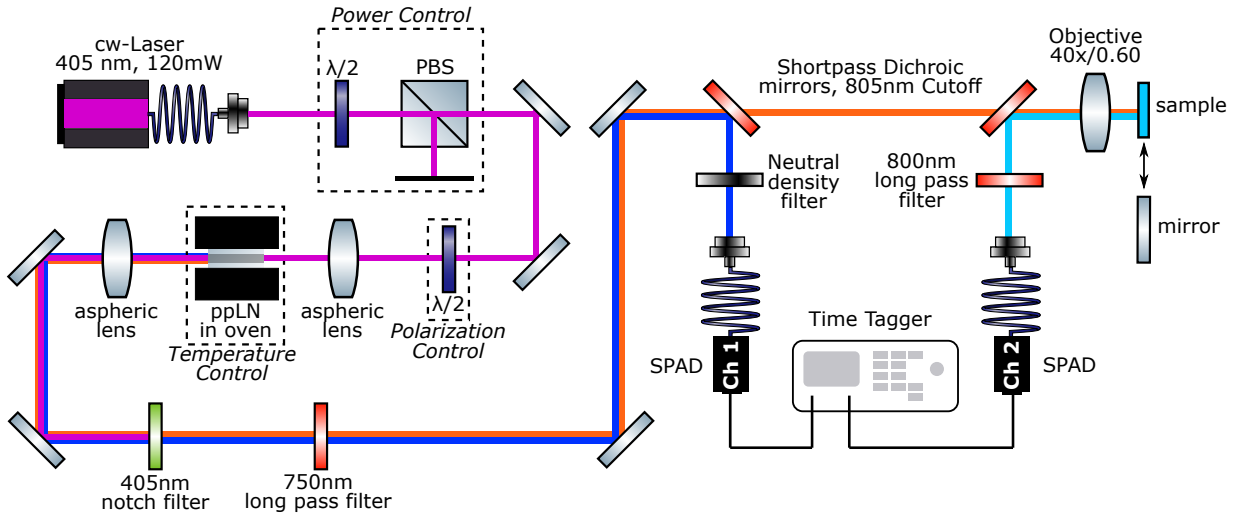


FIG. 2: Experimental Setup for the measurement of fluorescence lifetimes with time-frequency correlated photons. The left part shows the photon pair source, whereas the right side is the tailor-built microscope. Violet indicates the optical path of the pump, dark blue the heralding, orange the excitation and light blue the fluorescence beam.

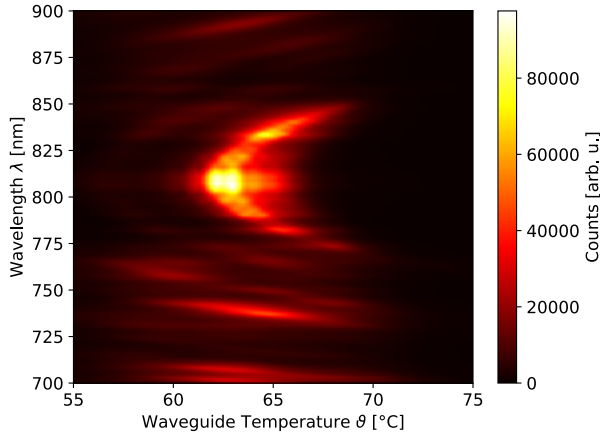


FIG. 3: Single photon spectrum of photon pair source depicted in fig. 2 for different waveguide temperatures ϑ

2. Averaging of $IRF(t)$ and $\tilde{F}(t)$ over the sets of measurement
3. Shift $IRF(t)$ so that $\mu_{IRF} = 0$ ps for all measurements.
4. Shift $\tilde{F}(t)$ equally to their corresponding $IRF(t)$
5. Normalize $IRF(t)$ and find value of σ_{IRF} by curve-fitting using eq. (4)
6. Find τ by curve-fitting of $\tilde{F}(t)$ using eq. (5)

IV. RESULTS

A. Integration Time

The averaged and background-corrected histograms for different integration times T are shown in fig. 4. As expected, the histogram peaks become more significant with longer integration times T . Furthermore, \tilde{F} is more noisy than IRF caused by the much lower coincidence count rate. However, the determined fluorescence lifetime of IR-140 is stabilized for longer integration times T at around 885 ps (fig. 5a) and its standard deviation drops into the range of 3 fs (fig. 5b).

But, it is remarkable that the values of τ diverge strongly for short integration times T . It is likely that this effect depends on the significance of the histogram and, thus, amount of detected coincidences. To gain a deeper understanding of this effect, the influence of the signal-to-noise ratio and the heralding efficiencies is investigated by inserting neutral density filters into the optical path of channel 1. The gained results are shown in the following subsection.

B. SNR and Heralding Efficiencies

Due to the background correction of all histograms, we use the following definition of the signal-to-noise ratio SNR [28].

$$SNR_{IRF} = \frac{IRF^{\max}}{\sigma_{IRF}} \quad (6)$$

$$SNR_{\tilde{F}} = \frac{\tilde{F}^{\max}}{\sigma_{\tilde{F}}} \quad (7)$$

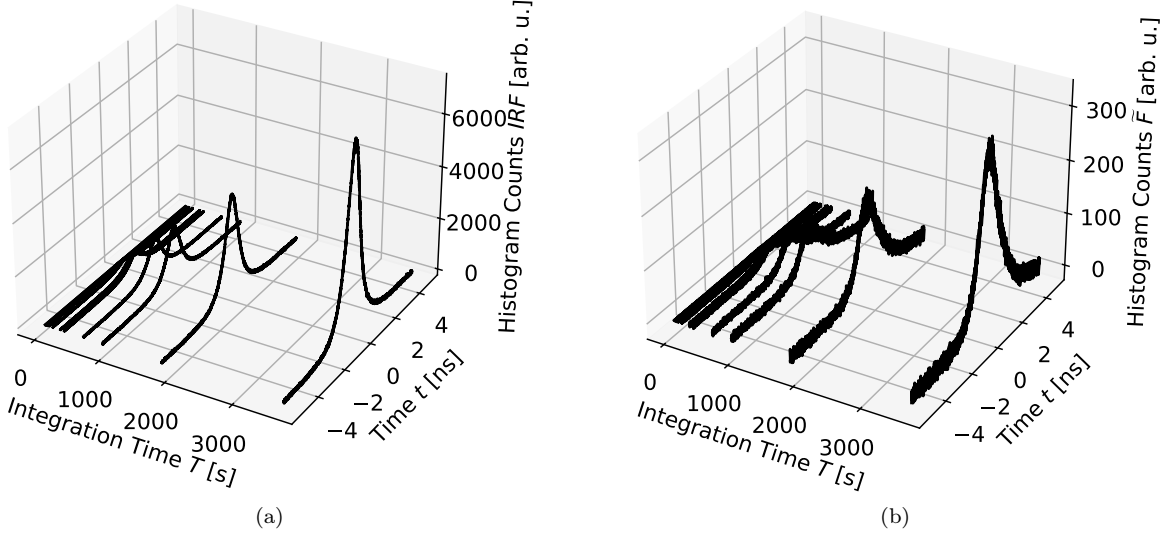


FIG. 4: IRF (4a) and \tilde{F} (4b) for different integration times T

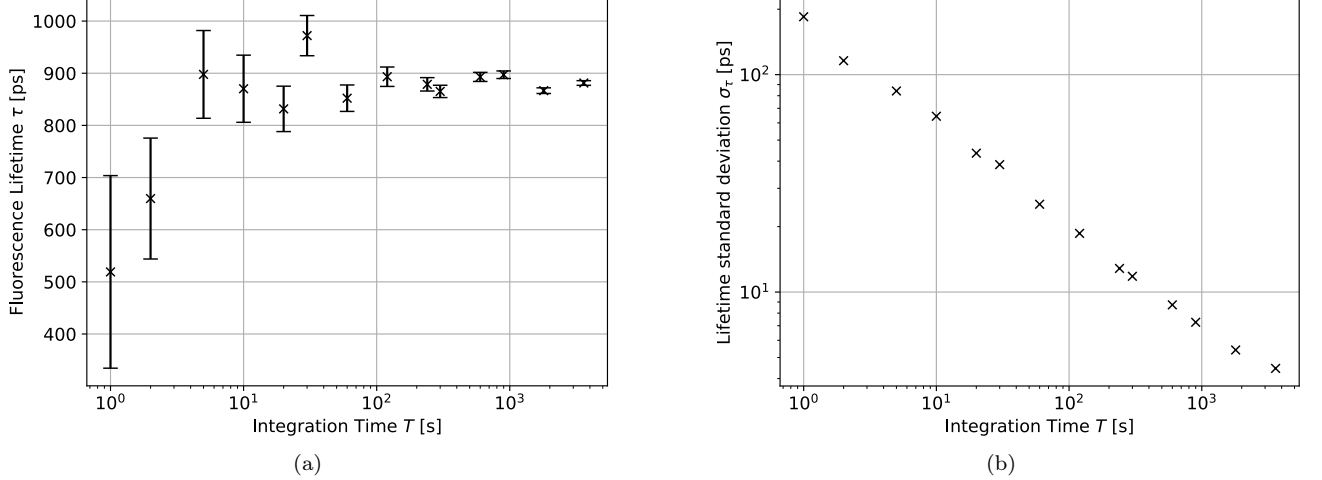


FIG. 5: Fluorescence lifetime τ (5a) and its standard deviation σ_τ (5b) depending on the integration time T

IRF^{max} and \tilde{F}^{max} represent the peak values of the non-normalized histograms. σ_{IRF} and $\sigma_{\tilde{F}}$ are the standard deviation of their background noise. Their estimation is based on the first $N_t = 300$ bins at times t_i of every recorded histogram, which corresponds to a time range of 600 ps. It ensures that all involved bins are related to the background noise and not to the relevant histogram range, which contains information about Δt or τ .

$$\sigma_{IRF} = \sqrt{\frac{1}{N_t} \cdot \sum_{i=0}^{N_t} IRF^2(t_i)} \quad (8)$$

$$\sigma_{\tilde{F}} = \sqrt{\frac{1}{N_t} \cdot \sum_{i=0}^{N_t} \tilde{F}^2(t_i)} \quad (9)$$

Fig. 6 shows the fluorescence lifetimes over the signal-to-noise ratio of instrument response function SNR_{IRF} (fig. 6a) and measured fluorescence $SNR_{\tilde{F}}$ (fig. 6b). In case of the instrument response function, τ becomes stable for $SNR_{IRF} \gtrsim 80$, whereas it is $SNR_{\tilde{F}} \gtrsim 9$ in case of the fluorescence measurement. Only the data point at $SNR_{\tilde{F}} \approx 13.1$, which corresponds to the measurement with a neutral density filter with optical density of 4.0, differs strongly. The reason for this is that no clear peak in the histogram was visible anymore and, thus, \tilde{F}^{max} represents the largest noise count in this case.

To conclude, fig. 6 shows that we can access a regime of reliable measurements, but with the clarity that the signal-to-noise ratio $SNR_{\tilde{F}}$ of the fluorescence detection is the most relevant criterion. This is evident since the amount of fluorescence photons is much lower than the

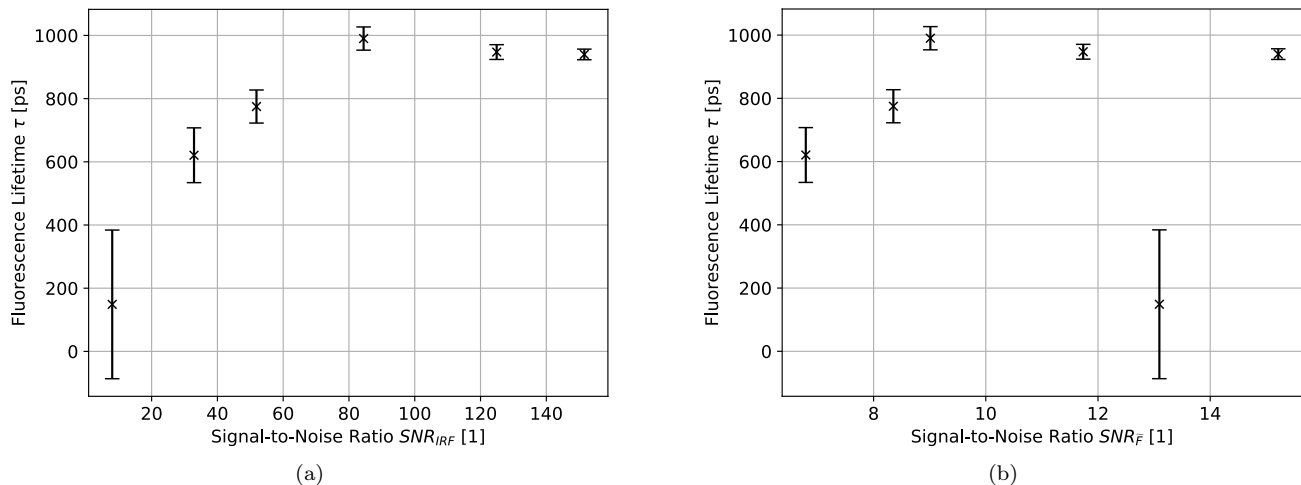


FIG. 6: Effect of the signal-to-noise ratios SNR_{IRF} (6a) and $SNR_{\tilde{F}}$ (6b) on fluorescence lifetime τ

amount of photons collected by the heralding detector or by the fluorescence detector during the measurement of the instrument response function.

The signal-to-noise ratio, which is a standard performance indicator in data processing, only gives information about required coincidence counts vs. accidental coincidences in the recorded histograms for reliable measurements. Since FLIM with correlated photon pairs is based on coincidence detection of two light beams, heralding efficiencies η may offer additional lower bounds on detection efficiencies and losses in light of reliable measurements. The heralding efficiencies $\eta_{1,2}$ are defined as ratio of measured coincidence rate R^{coin} to single count rates $R_{1,2}^{\text{single}}$ at detection channel 1 or 2.

$$\eta_{1,2} = \frac{R^{\text{coin}}}{R_{1,2}^{\text{single}}} \quad (10)$$

Fig. 7 illustrates the fluorescence lifetimes τ depending on the heralding efficiencies η_2 with regard to the photon counts R_2^{single} at the fluorescence detector (channel 2) for IRF and \tilde{F} . As visible, the values become stable for heralding efficiencies $\eta_2 \gtrsim 0.1\%$. In comparison, entangled photon pair sources usually show heralding efficiencies around 40% [29–31]. As a consequence, time-domain FLIM with time-frequency correlated photon pairs is feasible even if the initial heralding efficiency of a photon pair source cannot be reached because of the lossy conversion of one beam to fluorescence photons.

On the other side, the heralding efficiency η_1 with regard to heralding detection (channel 1) does not play an important role. As depicted in fig. 8, the fluorescence lifetime τ decreases with η_1 at certain points. Since in general the single photon rate R_1^{single} is much higher than R_2^{single} , its reduction, for example, by neutral density filters, has only little influence on the coincidence rate R^{coin} . For this reason, the heralding efficiency η_1

increases with higher optical densities, and τ shows the opposite behavior in comparison to fig. 7.

This technique shows promising potential for future application-oriented developments, including its suitability for advanced quantum-enhanced biological imaging. The current acquisition time of 15 min enables precise measurements; however, to make the approach more feasible for biomedical imaging applications requiring fast frame rates, enhancements in performance would be beneficial. Specifically, increasing the count rate of detected fluorescence in channel 2 relative to the heralding photons in channel 1 could be achieved through further optimization of the optical system. While increasing the SPDC generation rate via higher pump power might initially seem like a viable option, this approach requires careful consideration, as the linear increase in photon-pair rates can lead to detector saturation [25], resulting in artifacts and inaccuracies in fluorescence lifetime measurements. These insights provide a roadmap for advancing the method and enhancing its applicability in fast-paced imaging scenarios.

C. Spectroscopic Approach

Because of the usage of a waveguide source with a narrow bandwidth in comparison to usual photon pair sources based on nonlinear bulk crystals, a spectroscopic use case becomes conceivable. For this purpose, the waveguide temperature was varied to change the excitation wavelength according to fig. 3.

Fig. 9 shows the histograms IRF and \tilde{F} for different waveguide temperatures ϑ . In general, the counts are falling for increased temperature, which corresponds to the less amount of photons generated by the SPDC process for higher temperatures (see fig. 3). However, \tilde{F} shows a deviation from this general behavior: The

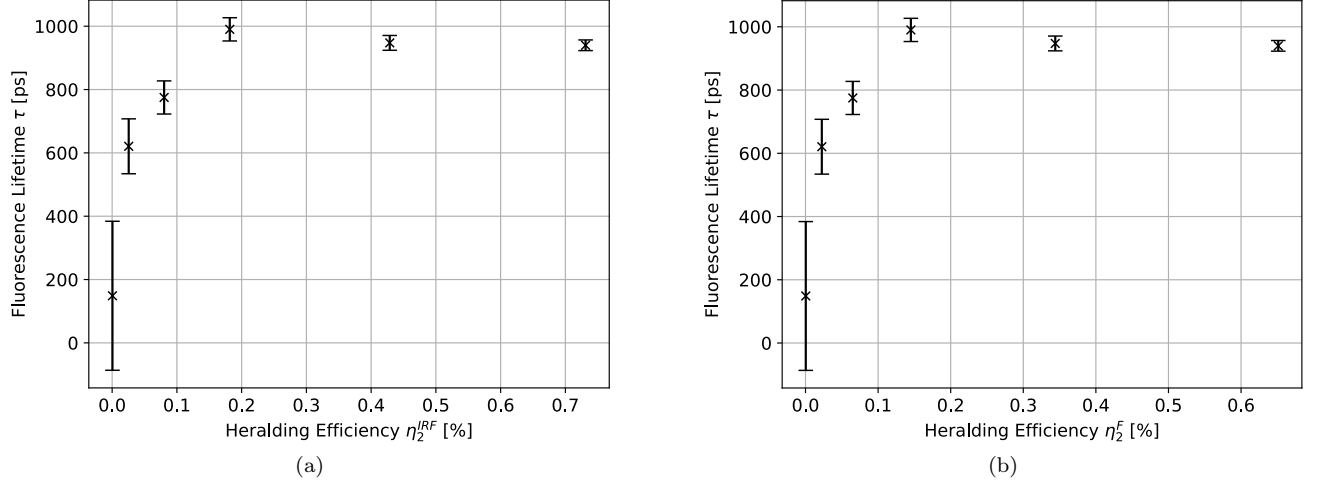


FIG. 7: Effect of the heralding efficiencies η_2^{IRF} (7a) and η_2^F (7b) regarding channel 2 (fluorescence detector) on fluorescence lifetime τ .

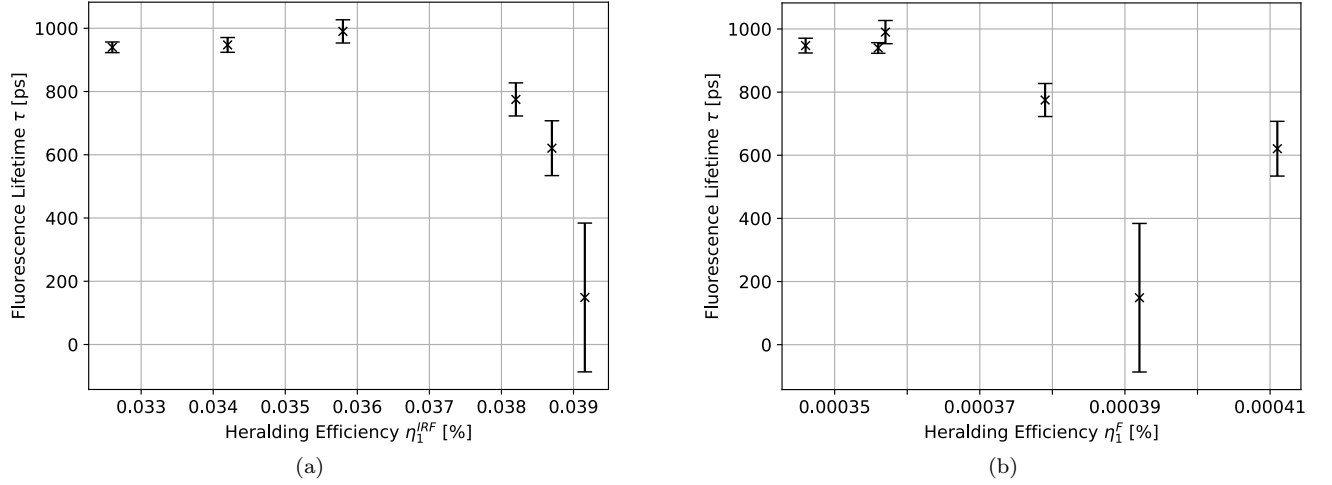


FIG. 8: Effect of the heralding efficiencies η_1^{IRF} (8a) and η_1^F (8b) regarding channel 1 (heralding detector) on fluorescence lifetime τ .

highest amount of coincidence counts appear at $\vartheta = 64^\circ\text{C}$. This indicates an optimum waveguide temperature ϑ where the combination of excitation wavelength and SPDC generation rate achieves the highest possible fluorescence rate.

The fluorescence lifetime τ measured by the setup of fig. 2 depending on the waveguide temperature ϑ or rather the excitation center wavelength λ_0 are shown by the black data points in fig. 10. A clear influence of λ_0 is not visible because nearly all values of τ are on the same level. This becomes obvious because no extraordinary energy transitions are known for IR-140, which would break Kasha's rule [34]. However, strong deviations arise for temperatures above 69°C . As in the case of short integration times T or low signal-to-noise ratios SNR , the histograms of IRF and \tilde{F} slowly become lost

in noise due to the reduced photon rates, which inhibit confidence in data evaluation.

D. Comparison with State-of-the-Art FLIM

Another notable point is the difference compared to the lifetimes measured by a state-of-the-art device (blue data points in fig. 10). This data was measured by a Leica Stellaris 8 with a multi-color laser and the HyD R detector. The data from the method using entangled photons have a mean value of $\langle\tau\rangle \approx 932$ ps, whereas the mean value measured by Leica Stellaris 8 is $\langle\tau\rangle \approx 818$ ps. Furthermore, the values of τ shown in sec. IV A and IV B also differ slightly. According to several publications, the fluorescence lifetime of IR-140 strongly varies depend-

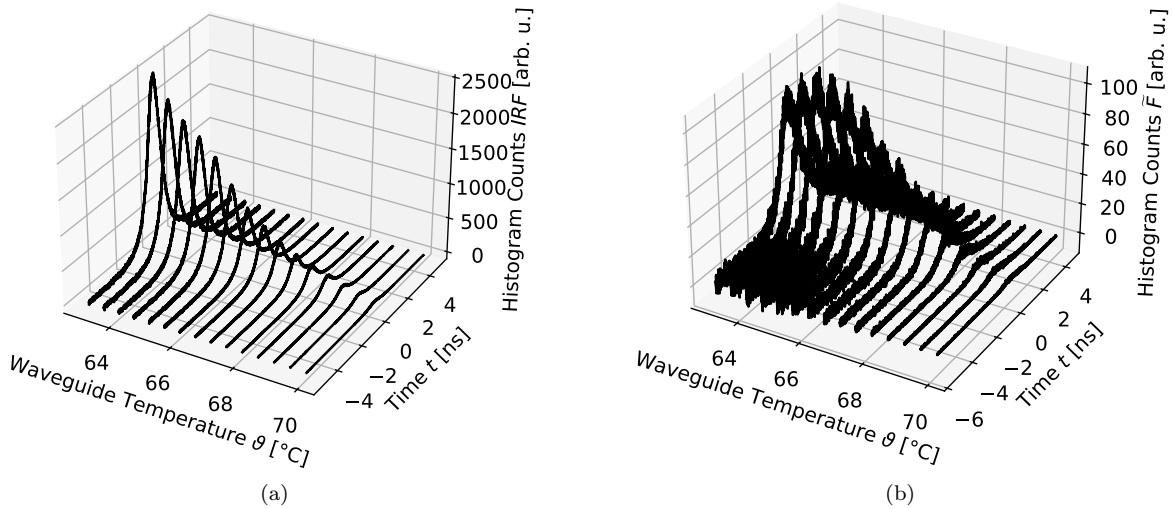


FIG. 9: IRF (9a) and \tilde{F} (9b) for different waveguide temperatures ϑ

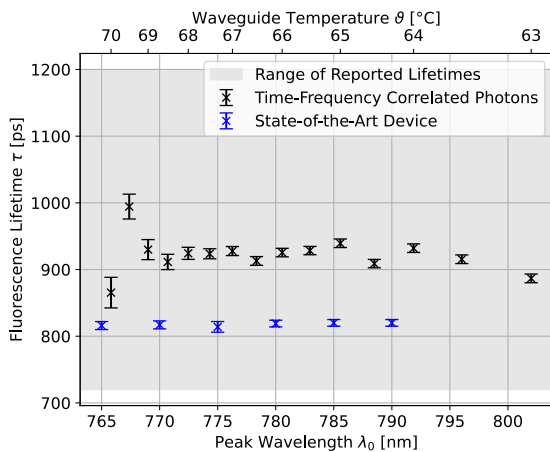


FIG. 10: Fluorescence lifetime τ depending on the waveguide temperature ϑ and the corresponding excitation center wavelength λ_0 . Black indicates data gained by the described method using entangled photons, while blue are comparative values measured by a state-of-the-art FLIM. The gray background visualizes the range of reported lifetimes [32, 33].

ing on the chemical environment between approximately 200 fs [35] and 1.2 ns [33]. A reported value more comparable to our sample of IR-140 solved in ethanol is 0.72 ns with excitation at 790 nm and fluorescence emission filtered by a (830 ± 10) nm-bandpass filter [32]. Consequently, these various data available in the literature indicate that the precise determination depends strongly on the experimental conditions, which may explain the differences in the shown data. Nevertheless, this variance also represents that FLIM using time-frequency correlated photons makes the monitoring of environmental influences possible.

However, both methods show results in the same order of magnitude. In light of the variability in lifetime τ reported in the available literature, this demonstrates their high comparability. This study highlights that the method using photon pairs can investigate such properties of fluorescence dyes, even though it is not yet fully technologically developed.

An important quantity in FLIM is the so-called figure-of-merit (also often called F-value) \mathcal{F} . It quantifies the sensitivity of a FLIM method in relation to the number of counts N [36].

$$\mathcal{F} = \frac{\sigma_\tau}{\tau} \cdot \sqrt{N} \quad (11)$$

In this definition of \mathcal{F} , N represents the sum of all counts in a background-corrected histogram \tilde{F} over all time bins t_i .

$$N = \sum_{i=0}^{N_i} \tilde{F}(t_i) \quad (12)$$

In an ideal measurement, \mathcal{F} is equal to unity, whereas real measurements show $\mathcal{F} > 1$.

Fig. 11 shows the figure-of-merit \mathcal{F} of the data related to the measurements for the spectroscopic approach. As visible, \mathcal{F} is substantially larger for the state-of-the-art FLIM. Since the values of τ and σ_τ in both methods are nearly identical, the different values of \mathcal{F} are mainly caused by the differences regarding N . This becomes reasonable with view to the different principles of classical time-domain FLIM and the method presented in this work. In classical FLIM, all fluorescence photons contributing to a recorded histogram are correlated to electronic heralding signals caused by laser pulses. However, for every single laser pulse, multiple fluorescence photons will be detected. In contrast to this, using correlated

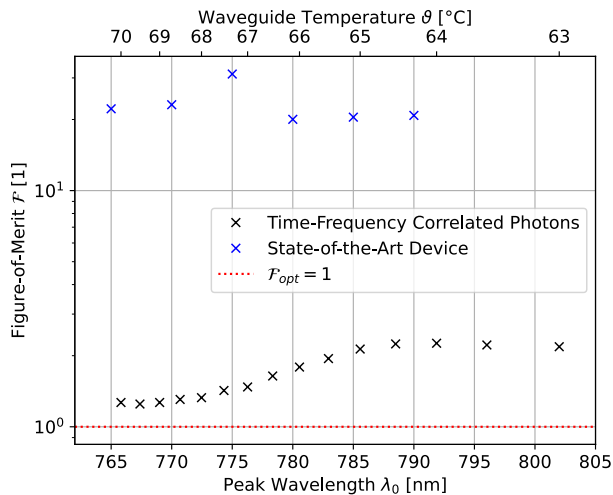


FIG. 11: Figure-of-merit \mathcal{F} depending on the waveguide temperature ϑ and the corresponding excitation center wavelength λ_0 . Black indicates data gained by the described method using entangled photons, while blue are comparative values measured by a state-of-the-art FLIM. The red dotted line represents the optimum of \mathcal{F} for an ideal measurement.

photon pairs, every detected fluorescence photon is associated with a single heralding photon. As a result, histograms recorded by coincidence measurements of photon pairs have fewer counts compared to histograms of classical time-domain FLIM, but these counts have higher significance since uncorrelated noise is not contributing. This finally results in a substantial improvement in the figure-of-merit \mathcal{F} .

In many protocols based on heralded single-photon sources measuring one photon of the pair, which results in twin photon collapse into a single-photon Fock state, ideally exhibits zero photon-number variance. Based on this, several quantum enhanced protocols have proved better-than-classical parameter estimation, for example, for absorption [37–39] or phase measurements [40, 41]. Accessing this quantum-enhanced regime may improve the presented method even more, but also requires low losses and high detection efficiencies [38]. For this reason, the implementation of such regime in FLIM with entangled photons might be challenging because of the inherent limits in single-photon fluorescence efficiency. Nevertheless, further investigations could provide more quantitative bounds to the quantum-enhanced regime.

V. CONCLUSION

We demonstrated several experimental limits of fluorescence lifetime determination using time-frequency correlated photons. For this purpose, continuous-wave pumped source based on SPDC was used. In principle, this method can be used with a minimum number of

photon pairs, which prevents the effect of photobleaching. Furthermore, considering the figure-of-merit demonstrates that measurement precision comparable to state-of-the-art devices is achievable. Only the rate of generated fluorescence photons and the integration time of the photon counting are crucial. Because of the narrow bandwidth of a waveguide-based photon pair source, it also allows a spectroscopic approach for the analysis of molecular properties without high equipment costs and, thus, represents a conceivable alternative to state-of-the-art methods for fluorescence lifetime spectroscopy and imaging.

For application-related cases in biology, chemistry or medicine, we suggest several improvements. For example, a photon pair source with more narrow bandwidth will enhance the wavelength-resolution. Also the imbalance between the rate of heralding and fluorescence photons has to be improved to increase the signal-to-noise ratios and heralding efficiencies, which will enable the shortening of the required integration times. Nevertheless, the functionality of this method can be further enlarged. A scanning approach as well as a ghost-imaging configuration can be easily implemented to gain image information of structured samples. Moreover, an amplitude modulation of the pump laser is embeddable to allow frequency-domain fluorescence lifetime measurements. With this, FLIM devices simultaneously operable in time- and frequency-domain are conceivable.

DATA AVAILABILITY STATEMENT

All data presented in this study, as well as the underlying data and python codes, are openly available on Zenodo (ref. [27]).

FUNDING

This research was funded by the Bundesministerium für Bildung und Forschung (BMBF), funding programs LIVE2QMIC (FKZ: 13N15954), QC4EP (FKZ: 13N16758) and Photonics Research Germany (FKZ: 13N15713 and 13N15717). It is integrated into the Leibniz Center for Photonics in Infection Research (LPI). The LPI, initiated by Leibniz Institute of Photonic Technology IPHT, Leibniz Institute for Natural Product Research and Infection Biology (Hans Knöll Institute) HKI, University Hospital Jena UKJ and Friedrich Schiller University Jena, is part of the BMBF national roadmap for research infrastructures. We also acknowledge the European Union’s Horizon 2020 Framework program Qu-Test (grant agreement ID 101113901) for financial support.

The Leica Stellaris 8 (used for the classical fluorescence measurements in fig. 10 and 11) is an integral part of the Microverse Imaging Center. For this, we acknowledge financial support by the Deutsche Forschungsgemeinschaft (DFG, German Research Foundation; Ger-

many's Excellence Strategy – EXC 2051 – Project-ID 390713860; project number 316213987 – SFB 1278; instrument funding ID 460889961 multi-photon laser scanning device).

AUTHOR CONTRIBUTIONS

Conceptualization: T.B.G.; Methodology: T.B.G. and V.F.G.; Investigation: T.B.G., N.J. and P.T.; Software: T.B.G.; Formal analysis: T.B.G.; Data curation: T.B.G.; Writing - original draft: T.B.G.; Writing - review and editing: all authors; Visualization: T.B.G.; Supervision: M.G. and V.F.G.; Project administration: T.B.G.; Funding acquisition: M.G. and C.E.

All authors have read and agreed to the published version of the manuscript.

ACKNOWLEDGMENTS

T.B.G. thank Nathan Harper and Scott K. Cushing (both California Institute of Technology) for fruitful discussions about the improvement of the microscope setup design and data processing.

T.B.G. thanks Kevin Lindt (TKFDM Data Steward) for support regarding topics of research data management.

We thank the Microverse Imaging Center (as well as Aurélie Jost and Sophie Neumann) for providing microscope facility support for data acquisition (and data analysis).

CONFLICTS OF INTEREST

The authors declare no conflict of interest.

-
- [1] M. Rumi and J. W. Perry, *Adv. Opt. Photon.* **2**, 451 (2010).
- [2] O. Krichevsky and G. Bonnet, *Reports on Progress in Physics* **65**, 251 (2002).
- [3] S. W. Hell and J. Wichmann, *Opt. Lett.* **19**, 780 (1994).
- [4] H. Blom and J. Widengren, *Chem. Rev.* **117**, 7377 (2017).
- [5] E. Matayoshi and A. Kleinfeld, *Biophysical Journal* **35**, 215 (1981).
- [6] J. Baumann, G. Calzaferri, and T. Hugentobler, *Chemical Physics Letters* **116**, 66 (1985).
- [7] S. Klitgaard, M. T. Neves-Petersen, and S. B. Petersen, *Journal of Fluorescence* **16**, 595 (2006).
- [8] W. Becker, A. Bergmann, and C. Biskup, *Microscopy Research and Technique* **70**, 403 (2007).
- [9] J.-P. Knemeyer, N. Marmé, and J. D. Hoheisel, *Analytical and Bioanalytical Chemistry* **387**, 37 (2007).
- [10] D. Chorvat Jr. and A. Chorvatova, *Laser Physics Letters* **6**, 175 (2009).
- [11] A. Gerega, N. Zolek, T. Soltysinski, D. Milej, P. Sawosz, B. Toczylowska, and A. Liebert, *Journal of Biomedical Optics* **16**, 067010 (2011).
- [12] P. Tinnefeld, D.-P. Herten, and M. Sauer, *J. Phys. Chem. A* **105**, 7989 (2001).
- [13] N. Harper, B. P. Hickam, M. He, and S. K. Cushing, *J. Phys. Chem. Lett.* **14**, 5805 (2023).
- [14] A. Eshun, X. Yi, A. Wilson, S. Jeppson, J. H. Yoo, S. Kiannejad, M. Rushford, T. Bond, and T. Laurence, *Opt. Express* **31**, 26935 (2023).
- [15] M. Y. Berezin and S. Achilefu, *Chemical reviews* **110**, 2641 (2010).
- [16] W. Becker, *Journal of microscopy* **247**, 119 (2012).
- [17] P. Chen, Q. Kang, J. Niu, Y. Jing, X. Zhang, B. Yu, J. Qu, and D. Lin, *Biomed. Opt. Express* **14**, 1718 (2023).
- [18] C. Couteau, *Contemporary Physics* **59**, 291 (2018).
- [19] A. Fedrizzi, T. Herbst, A. Poppe, T. Jennewein, and A. Zeilinger, *Opt. Express* **15**, 15377 (2007).
- [20] R. d. J. León-Montiel, J. c. v. Svozilík, J. P. Torres, and A. B. U'Ren, *Phys. Rev. Lett.* **123**, 023601 (2019).
- [21] M. Fiorentino, S. M. Spillane, R. G. Beausoleil, T. D. Roberts, P. Battle, and M. W. Munro, *Opt. Express* **15**, 7479 (2007), spontaneous Parametric Down-conversion.
- [22] G. Fujii, N. Namekata, M. Motoya, S. Kurimura, and S. Inoue, *Opt. Express* **15**, 12769 (2007).
- [23] P. Abolghasem, M. Hendrych, X. Shi, J. P. Torres, and A. S. Helmy, *Opt. Lett.* **34**, 2000 (2009).
- [24] S. M. Spillane, M. Fiorentino, and R. G. Beausoleil, *Opt. Express* **15**, 8770 (2007).
- [25] T. B. Gäbler, P. Hendra, N. Jain, and M. Gräfe, *Advanced Physics Research* **3**, 2300037 (2024).
- [26] R. Pollmann, F. Roeder, V. Quiring, R. Ricken, C. Eigner, B. Brecht, and C. Silberhorn, *Opt. Express* **32**, 23945 (2024).
- [27] T. B. Gäbler, N. Jain, P. Then, C. Eggeling, M. Gräfe, and V. F. Gilli, “Benchmarking of fluorescence lifetime measurements using time-frequency correlated photons,” *Zenodo* (2025), <https://doi.org/10.5281/zenodo.14654235>.
- [28] V. F. Gili, C. Piccinini, M. Safari Arabi, P. Kumar, V. Besaga, E. Brambila, M. Gräfe, T. Pertsch, and F. Setzpfandt, *Applied Physics Letters* **121**, 104002 (2022).
- [29] S. Ramelow, A. Mech, M. Giustina, S. Gröblacher, W. Wieczorek, J. Beyer, A. Lita, B. Calkins, T. Gerrits, S. W. Nam, A. Zeilinger, and R. Ursin, *Opt. Express* **21**, 6707 (2013).
- [30] F. Steinlechner, M. Gilaberte, M. Jofre, T. Scheidl, J. P. Torres, V. Pruneri, and R. Ursin, *J. Opt. Soc. Am. B* **31**, 2068 (2014).
- [31] E. Brambila, R. Gómez, R. Fazili, M. Gräfe, and F. Steinlechner, *Opt. Express* **31**, 16107 (2023).
- [32] C. L. Hutchinson, T. L. Troy, and E. M. Sevick-Muraca, *Appl. Opt.* **35**, 2325 (1996).
- [33] D. J. S. Birch, G. Hungerford, and R. E. Imhof, *Review of Scientific Instruments* **62**, 2405 (1991).

- [34] J. C. del Valle and J. Catalán, *Phys. Chem. Chem. Phys.* **21**, 10061 (2019).
- [35] D. Wang, J. Xiang, H. Jiang, G. Xu, and Q. Gong, *Journal of Optics A: Pure and Applied Optics* **5**, 123 (2003).
- [36] H. C. Gerritsen, M. A. H. Asselbergs, A. V. Agronskaia, and W. G. J. H. M. Van Sark, *Journal of Microscopy* **206**, 218 (2002).
- [37] G. Brida, M. Genovese, and I. Ruo Berchera, *Nature Photonics* **4**, 227 (2010).
- [38] R. Whittaker, C. Erven, A. Neville, M. Berry, J. L. O'Brien, H. Cable, and J. C. F. Matthews, *New Journal of Physics* **19**, 023013 (2017).
- [39] J. Sabines-Chesterking, A. R. McMillan, P. A. Moreau, S. K. Joshi, S. Knauer, E. Johnston, J. G. Rarity, and J. C. F. Matthews, *Opt. Express* **27**, 30810 (2019).
- [40] A. Kuzmich and L. Mandel, *Quantum and Semiclassical Optics: Journal of the European Optical Society Part B* **10**, 493 (1998).
- [41] L. Pezzé and A. Smerzi, *Phys. Rev. Lett.* **100**, 073601 (2008).